Characterization of the Solar Power Resource in Europe and Assessing Benefits of Co-Location with Wind Power Installations

Cedric Bozonnat and C. Adam Schlosser

MIT JOINT PROGRAM ON THE SCIENCE AND POLICY of GLOBAL CHANGE

Report No. 268
October 2014

The MIT Joint Program on the Science and Policy of Global Change combines cutting-edge scientific research with independent policy analysis to provide a solid foundation for the public and private decisions needed to mitigate and adapt to unavoidable global environmental changes. Being data-driven, the Program uses extensive Earth system and economic data and models to produce quantitative analysis and predictions of the risks of climate change and the challenges of limiting human influence on the environment—essential knowledge for the international dialogue toward a global response to climate change.

To this end, the Program brings together an interdisciplinary group from two established MIT research centers: the Center for Global Change Science (CGCS) and the Center for Energy and Environmental Policy Research (CEEPR). These two centers—along with collaborators from the Marine Biology Laboratory (MBL) at Woods Hole and short- and long-term visitors—provide the united vision needed to solve global challenges.

At the heart of much of the Program's work lies MIT's Integrated Global System Model. Through this integrated model, the Program seeks to: discover new interactions among natural and human climate system components; objectively assess uncertainty in economic and climate projections; critically and quantitatively analyze environmental management and policy proposals; understand complex connections among the many forces that will shape our future; and improve methods to model, monitor and verify greenhouse gas emissions and climatic impacts.

This reprint is one of a series intended to communicate research results and improve public understanding of global environment and energy challenges, thereby contributing to informed debate about climate change and the economic and social implications of policy alternatives.

Ronald G. Prinn and John M. Reilly,
Program Co-Directors

For more information, contact the Program office:
MIT Joint Program on the Science and Policy of Global Change

Postal Address:
Massachusetts Institute of Technology
77 Massachusetts Avenue, E19-411
Cambridge, MA 02139 (USA)

Location:
Building E19, Room 411
400 Main Street, Cambridge

Access:
Tel: (617) 253-7492
Fax: (617) 253-9845
Email: ***globalchange@mit.edu***
Website: ***http://globalchange.mit.edu/***

Characterization of the Solar Power Resource in Europe and Assessing Benefits of Co-Location with Wind Power Installations

Cedric Bozonnat[*†] and C. Adam Schlosser[*]

Abstract

The extent, availability and reliability of solar power generation are assessed over Europe, and—following a previously developed methodology—special attention is given to the intermittency of solar power. Combined with estimates of wind power resource over Europe from a companion assessment, we assess the benefits of co-location of solar and wind power installations, particularly with respect to aggregate power generation and local mitigation of intermittency. Consistent with previous studies, our results show that the majority of solar potential is found in southern Europe, which also displays the strongest availability. We also found that higher latitude locations, around central Europe, benefit from medium to high solar power during the warm season. If a region's availability of solar power is sufficient—as determined by a minimum technological threshold for photovoltaic extraction— it possesses the potential to reduce intermittency by aggregation and interconnection. We find these conditions occurring to a moderate extent over mainland central Europe. Finally, the result of co-location of wind and solar power is increased power availability over the whole continent, especially in central Europe where neither resource is strong. In terms of local intermittency mitigation, the regions that benefit most are the Mediterranean and Baltic countries.

Contents

[*] Joint Program on the Science and Policy of Global Change, Massachusetts Institute of Technology, MA, USA.
[†] Corresponding author (Email: cedric.bozonnat@gmail.com)

1. INTRODUCTION

Interest in renewable energies has been growing over the past few years in Europe. The European Commission's "Three-Twenties" project set targets in 2007 to reach a low-carbon and energy-efficient economy by 2020: the aim is to improve energy efficiency by 20%, to diminish European greenhouse gas emission by 20% from 1990 levels and to increase the share of energy consumption from renewable sources to 20%. The goals differ from one country to another, depending on their resources, current levels of renewables, and economic welfare. Some countries (e.g., Germany) have stimulated Photovoltaic (PV) growth in order to reach the target percentage they have been assigned, stating clearly in their policies their will to "go green". However, other European regions are still struggling to make use of their solar power resource, and lack potential for a portfolio of renewable energy generation with other technologies such as wind.

PV technology does not represent the highest share in the European renewable energies portfolio; however, it is the technology with the most potential for growth. In 2006, according to the European Commission (2009), the total PV capacity installed in the European Union was about 3 GW, which increased more than five times by 2009, to a total cumulative capacity of 16.8 GW. Facing the impressive progress made by the PV sector, a clear assessment of the solar resource over Europe is needed. Besides knowing where the most productive solar resources lie, it is also crucial to better understand and quantify its intermittency—a key feature of solar resource—as a guide toward sound and strategic widespread deployment.

Recently, Cosseron *et al.* (2014) and Kriesche and Schlosser (2014) assessed wind power resource and its intermittency in Europe, identifying areas with the most productive wind power sources and defining wind intermittency. Wind and solar power generation face strong seasonal changes: wind potential is stronger in winter than in summer, whereas solar exhibits stronger potential in summer than in winter. In this regard, the combination of wind and solar power could counterbalance the effects of intermittency, leveling the seasonal variation. Future European power supply systems are expected to be heavily reliant on renewables (predominantly wind and solar), and the quantification of their intermittency and the potential for its mitigation can serve as valuable and actionable information for strategic deployment options—such as the connection of solar and wind farms throughout inter EU-nation grids, or the co-location of solar and wind power installations to counterbalance seasonal changes.

The aim of this report is primarily to provide an assessment of solar power over Europe, following a methodology developed by Gunturu and Schlosser (2011). The data used to compute solar power is described in Section 2, as well as the methodology of assessing solar power. In Sections 3 and 4, we provide results of our analyses on solar power availability. Section 5 focuses then on the secondary aim of this report, which is to study the potential mitigation of intermittency impacts through co-located solar and wind power over Europe.

2. METHODOLOGY

2.1 Data

Our goals are to assess solar potential over Europe and to quantify the benefits of co-location of wind and solar power. To achieve this, an evaluation of global irradiation, cloud cover and wind power density over Europe is required. High-resolution time and spatial data is required because of the spatio-temporal variability of wind and solar resources with respect to meteorological and climate scale phenomenon and the need of power management and deployment to resolve sub-diurnal features. Additionally, in order to compute representative and significant statistics over the seasons, a multi-decadal timespan of data is required.

To meet these conditions, we use the Modern-Era Retrospective Analysis for Research and Applications (MERRA) data. The MERRA data of Rienecker *et al.* (2011) has a spatial resolution of ½° (lat) × ⅔° (lon) and a time resolution of one hour. The data set spans over 31 years, from January 1979 to December 2009. The MERRA database, constructed at the NASA Center for Climate Simulation, reconstructs the atmospheric state by assimilating observational data from different platforms into a global model. The aim of MERRA is to provide a more accurate data set using a comprehensive suite of satellite-based information for climate and atmospheric research.

The present data set has been developed with GEOS-5 ADAS (version 5.2.0). The system consists of the GEOS-5 model and the Grid-point Statistical Interpolation (GSI) analysis. The Global Modeling and Assimilation Office (GMAO) and the National Oceanic Atmospheric Administration (NOAA) have developed GSI jointly. In the analyses that follow, we consider various metrics across a range of time-filter windows:

- Whole data: all available hourly data
- Cold Season: data restricted to the months October–March
- Warm Season: data restricted to the months April–September

2.2 Solar Power

In order to evaluate solar irradiation from the MERRA data construction, we provide a quick overview of the transmittance-reflectance correlations method, as described in Hammer *et al.* (2003). Solar irradiation is constrained by four main factors. First, the earth's geometry, revolution and rotation: a correction factor (also named eccentricity factor, depending on the sun angle) is applied to take into account the varying solar distance. Second, the atmospheric attenuation: solar radiations are attenuated by gases, liquid and solid particles (the attenuation by gas constituents is described by the optical air mass and the optical thickness; the attenuation by liquid and solid particles is given by the Linke Turbidity). Third, the cloud attenuation: due to lack of coverage through ground measures, cloud cover is assessed from satellite observation; the reflected irradiance is measured and correlated to cloud transmission. Fourth is the terrain: elevation, shadow, surface orientation and inclination. Terrain is estimated by Suri *et al.* (2005) by using a Geographical Information System coupled with the satellite observations.

Once terrestrial solar irradiation is computed, it is divided in three components. Radiation selectively attenuated by the atmosphere that reaches the Earth's surface directly (without being reflected or scattered) is called *direct radiation*, and represents the biggest share. The second component of the global radiation is scattered light, called *diffuse radiation*. The third and smallest component is the reflected radiation at the surface. PV technology is able to capture all three components, but the reflected radiation on the ground will be neglected in this study (as in Suri and Hofierka, 2004).

We use the following MERRA data sets:

- Surface Incident Shortwave Flux
- Surface Downward Photosynthetic Available Radiation (PAR) Direct Flux
- Surface Downward PAR Diffuse Flux

The first data set consists of photons with wavelengths ranging from 300–2500 nm (ultraviolet to infrared). However, current PV cells are not able to use the entire range of wavelengths, due to the bandgap intrinsic to every PV material (Conibeer, 2007). The bandgap of a semiconductor is the minimum energy required to excite an electron into a free state from a bound state; therefore, only a photon with energy higher than the bandgap could be absorbed. Moreover, the excess energy of photons with energy higher than the bandgap is not effectively used; this is called thermalization. These two power-loss mechanisms apply to single-bandgap cells, such as crystalline silicon cells (c-Si) with a bandgap energy of approximately 1.1 eV. The inability to absorb the photons with energy less than the bandgap, and the thermalization of photon energies exceeding it, significantly reduce the amount of usable incident solar energy—to approximately 50% (Huang and Han, 2012). We will therefore refer to this 50% of the surface incident shortwave flux as the *total irradiation useable for PV*.

2.3 Electricity Generation

Once potential solar power is assessed, we focus on the actual electricity generation from PV. For a baseline estimate, we look at PV panels mounted on a horizontal plane. We calculate the electricity generated from a PV system using the same equation as Suri *et al.* (2007):

$$E = P_k \; P_R \; G \tag{1}$$

Where E (kWh) is the electricity generated, P_k is the unit peak power (assumed to be $1kW_p$ (kiloWattPeak) in our calculation), P_R is the performance ratio measuring the efficiency of the components other than the modules, and G is the yearly sum of total irradiation useable on the horizontal PV module (kWh/m^2). We assume a value of 0.75 for the performance ratio, which is typical for a mono- or poly-crystalline silicon PV panel—currently the most widespread technologies, according to Suri *et al.* (2007).

Equation (1) is derived from equation (2):

$$E = G\ S\ \eta \tag{2}$$

with

$$\eta = \frac{E_{Elec}}{E_{Light}} = \eta_{system}\ \eta_{stc} = P_R\ \eta_{stc} \tag{3}$$

η is the global efficiency of the solar panel and can be divided in two parts: η_{system}, which is the performance ratio defined above, and η_{stc} which is the efficiency in the standard test conditions (Irradiation 1000 W/m^2, Temperature 25°C) and corresponds to the efficiency of the modules. η_{stc} could therefore be defined as the efficiency with an input $G_{stc} = 1000\ W/m^2$ (standard test conditions) and an output P, the peak power, depending on the technology. The peak power, also called nominal power, is the theoretical output in the standard test conditions. The unit peak power, P_k, is then derived from the peak power as following:

$$\eta_{stc} = \frac{P}{G_{stc}\,S} = \frac{P_k}{S} \tag{4}$$

At this point, equation (1) is easily derived from equation (2):

$$E = G\ S\ P_R\ \frac{P_k}{S} = G\ P_R\ P_k \tag{5}$$

3. CHARACTERIZATION OF SOLAR POWER RESOURCE

3.1 Mean and Median

Figures 1a and 1b show the mean and median (respectively) solar irradiation useable for PV averaged over the sunshine duration (from sunrise to sunset) for the years 1979–2009. Blank areas in these figures indicate where the solar power is below 80 W/m^2. This cut-off value refers to the minimum solar power required for electricity production and is based on Ubertini and Desideri (2002). They have noted a cut-off value ranging from 20 to 80 W/m^2. We have chosen the upper bound; as such, our study is a conservative estimate of solar resource in this context.

At first glance, solar power seems harvestable (i.e. useable for PV) everywhere except for the extreme northern part of the Scandinavian countries. However, looking at the median values (Figure 1b), we find that solar power is harvestable less than half of the time over northern parts of Europe, including Great Britain, northern France and Iceland, as well as the Baltic region (Estonia, Latvia and Lithuania) and Scandinavian countries. Generally, the median values are lower than the mean values; this difference is most apparent in northern regions of our domain of interest. This characteristic indicates that there are strong but infrequent episodes of harvestable solar irradiation. This intermittency will be analyzed further in the sections that follow.

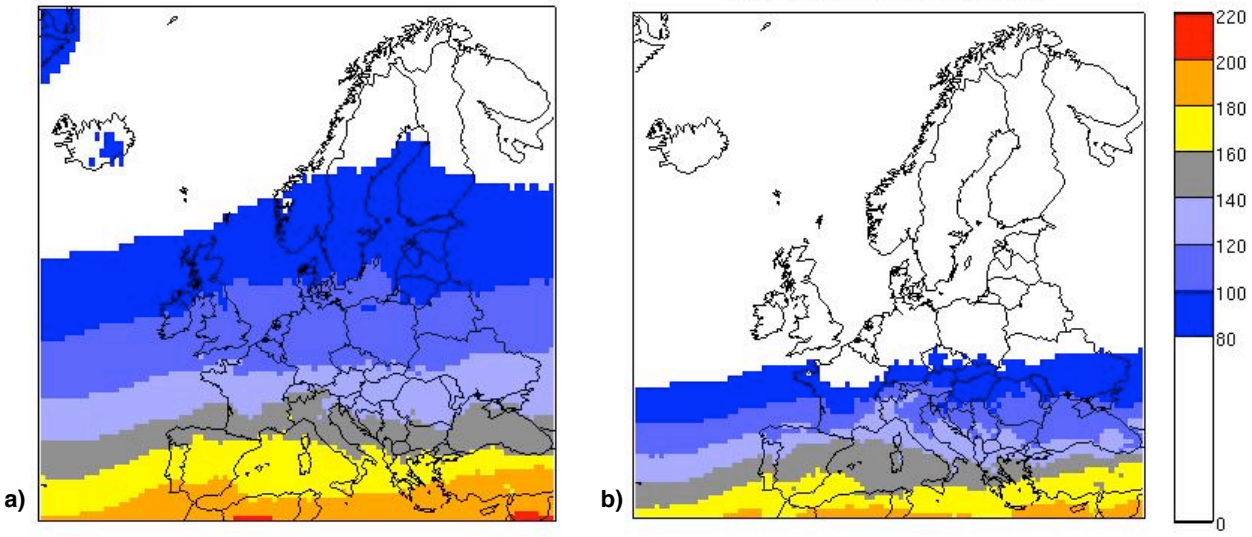

Figure 1. Geographical variation of the mean (a) and median (b) solar irradiation (W/m^2) useable for PV, averaged over the sunshine duration.

Another feature of solar power is its strong seasonal tendencies. Lack of harvestable solar power in the northern part of the Scandinavian countries is largely attributed to very low values of solar irradiation during the cold season. **Figures 2a and 2b** display respectively the mean solar irradiation useable for PV during the cold and the warm seasons, averaged over the sunshine duration. During the cold season, only lower latitude regions (south of France) show a mean availability of harvestable solar power. However, during the warm season, solar power is available everywhere—even in the northern part of the Scandinavian countries. Thus, two main areas appear: one where solar power is harvestable all year long, and one where solar potential is insufficient during the cold season.

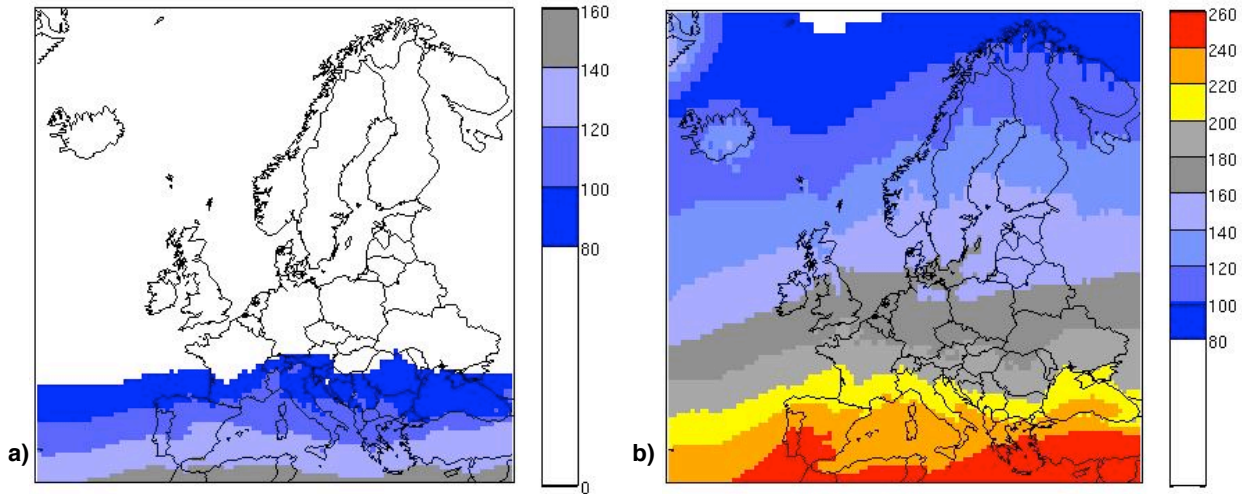

Figure 2. Geographical variation of the mean solar irradiation (W/m^2) useable for PV during the cold season (a) and the warm season (b), averaged over the sunshine duration.

As stated in Chenni *et al.* (2011), PV technology can use the direct and diffuse portions of solar irradiation and thus, even in overcast conditions, a PV system could still provide electricity

as long as the diffuse solar irradiation is above the cut-off value. We show in **Figure 3** the PAR direct and diffuse portions of solar irradiation, averaged over the sunshine duration. Note that the areas with no shading no longer represent the values under the cut-off, as in Figure 1.

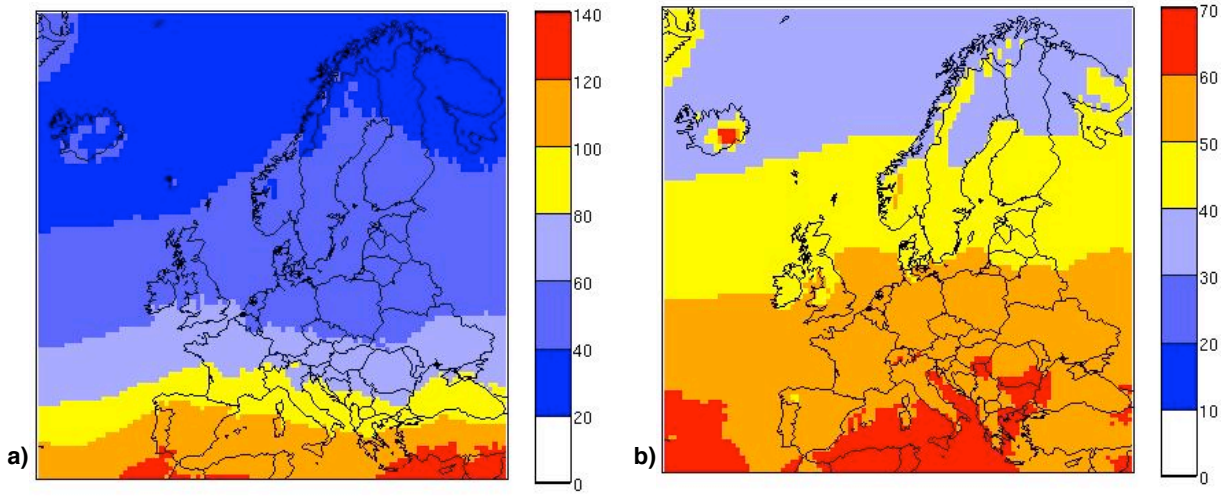

Figure 3. Geographical variation of the mean PAR direct irradiation (a) and PAR diffuse irradiation (b), averaged over the sunshine duration. Units are in W/m^2.

Since PV cells respond to more than the PAR portion of the solar spectrum, the total direct and diffuse solar irradiation useable for PV is greater than what is displayed on Figure 3. These figures are useful since they provide a first-order overview of the ratio of direct to diffuse irradiation. The percentage of diffuse solar irradiation is greater in higher latitudes and cloudier conditions than in lower latitudes and sunnier conditions. For example, the mean PAR direct irradiation in Spain is about 110 W/m^2 when the mean PAR diffuse irradiation is around 55 W/m^2, accounting for 25% of the total PAR irradiation. In Scotland, the mean PAR direct irradiation is about 50 W/m^2 while the mean PAR diffuse irradiation is about 45 W/m^2—nearly 50% of the total PAR irradiation.

3.2 Evaluation of Resource Estimates

3.2.1 Comparison with Hammer et al. (2003)

We consider here the results of Hammer *et al.* (2003) who worked with data from METEOSAT satellite. The global solar radiation (shortwave flux) data, which covers a 2-year period (1996 and 1997), with a 30-minute time resolution and a 10 km spatial grid, was constructed with the HELIOSAT method, originally proposed by Cano *et al.* (1986) and later modified by Hammer *et al.* (1998). The main idea of the HELIOSAT method in constructing a solar irradiation database from satellite images is to deal separately with atmospheric and cloud extinction (as described in Section 2.2). The three main steps are 1) the calculation of a clear sky irradiation map, 2) computation of a cloud index, and 3) derivation of the real sky irradiation (reducing the clear sky irradiation by taking into account the cloud index). The details of the

algorithm are described in Hammer *et al.* (1998) and some improvements of the method are also explained in Hammer *et al.* (2003).

Figure 4 and **Figure 5** show that solar power decreases with latitude. Southern portions of France, Italy and regions south of Spain show strong solar potentials—above 350 W/m^2. With few exceptions, the maximum and minimum values between Hammer and MERRA are consistent; the main patterns, which primarily track with latitude, are also consistent. We note that the Hammer estimates are based on two years of data and are unavailable as gridded data; therefore our comparisons are limited to qualitative remarks.

Figure 4. Geographical variation of the annual mean shortwave flux based on the years 1996 and 1997, averaged over the sunshine duration. Units are in W/m^2. (Source: Hammer *et al.* (2003), Figure 5).

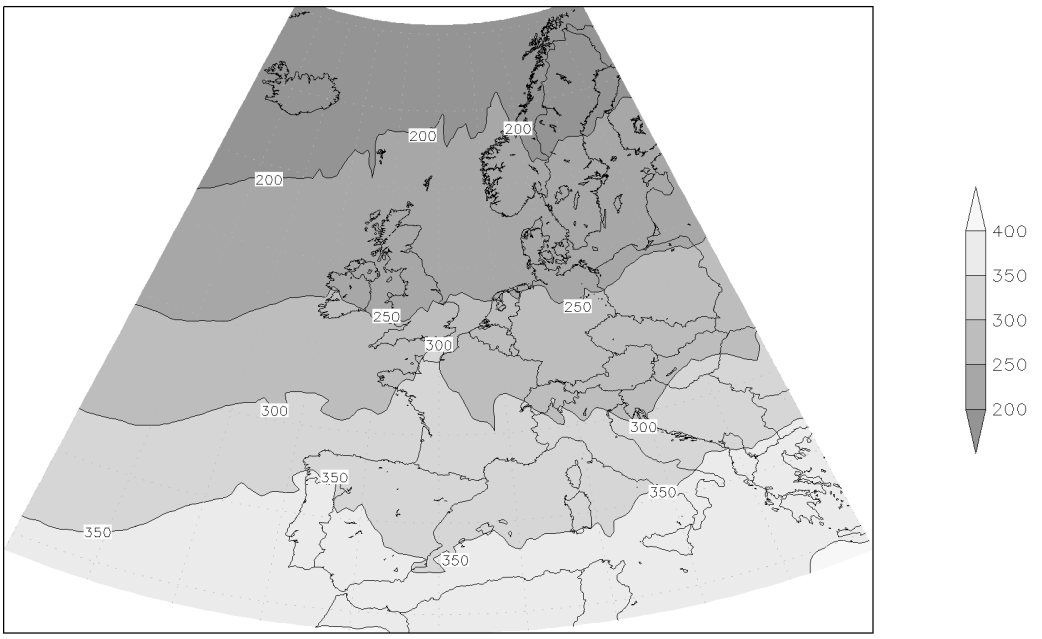

Figure 5. Geographical variation of the annual mean shortwave flux based on the years 1996 and 1997, averaged over the sunshine duration, computed with MERRA data and using the same color scale as Hammer *et al.* (2003). Units are in W/m^2.

3.2.2 Comparison with Suri et al. (2007)

The data used by Suri *et al.* (2007) was developed from the Photovoltaic Geographic Information System (PVGIS) and ground measurements from 566 meteorological stations over Europe. The database covers 10 years from 1981 to 1990 with a spatial resolution of 1 km × 1 km and includes monthly averages. **Figures 6 and 7** present the yearly sum of electricity generation from a 1 kW_p horizontal PV system, calculated using equation (1).

In southern Europe, results obtained from MERRA are quite similar to that of Suri *et al.* (2007). Their results show more texture due to the fine spatial resolution used, but our results are still consistent: south of France, north of Italy, north of Spain and Greece display values around 1000 and 1100 kWh/kW_p; Portugal, south of Spain, south of Italy and the Mediterranean Sea reach values ranging from 1100 to 1300 kWh/kW_p. As noted by Suri *et al.* (2007), "the highest potential for solar electricity generation is in Portugal and in the Mediterranean region with strong peaks in cloudless summer."

For central Europe, at intermediate latitudes both data sets are still consistent, with a PV potential in the range of 700–1000 kWh/kW_p. However, the comparison reveals distinctions for northern Europe. Computed with the MERRA data, the regions with poorest solar potential are the Scandinavian countries, Scotland, the Baltic region and Iceland, where the yearly generation falls under 700 kWh/kW_p. The results from Suri *et al.* (2007) show better potential for the Baltic countries and South Sweden and Finland, where the expected yearly generation is maintained between 700 and 800 kWh/kW_p. As in Hammer *et al.* (2003), the comparison above only aims at qualitative remarks, as the Suri *et al.* (2007) data also uses a different spatial and time resolution.

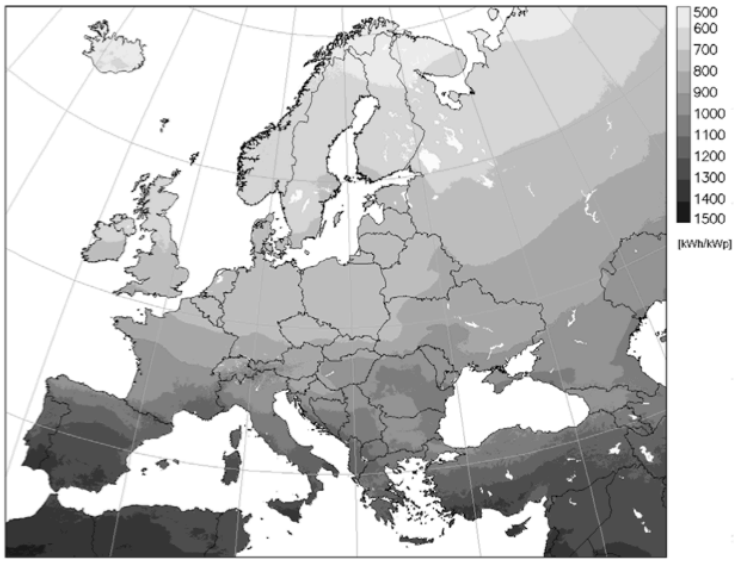

Figure 6. Geographical variation of the yearly sum of electricity generation from a 1 kW_p PV configuration with modules at horizontal position based on the years 1981 to 1990. Units in kWh/kW_p. (Source: Suri *et al.* (2007), Figure 1a).

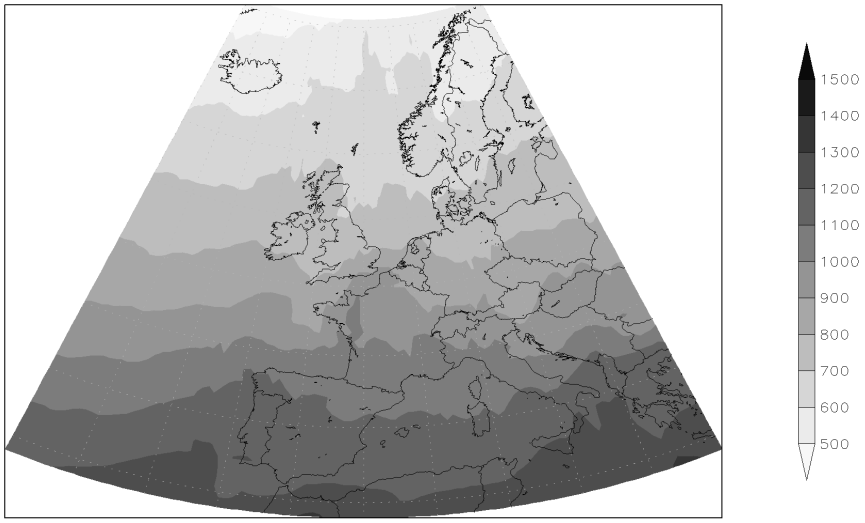

Figure 7. Geographical variation of the yearly sum of electricity generation from a 1 kW_p PV configuration with modules at horizontal position based on the years 1981 to 1990, computed with MERRA data and using the same color scale as Suri *et al.* (2007). Units in kWh/kW_p.

3.3 Cloud Cover

Since calculation of the solar irradiation depends on cloud cover, it is crucial to also assess cloud cover over Europe from MERRA data. **Figures 8a and 8b** show respectively the mean and median cloud cover, averaged over 31 years over the sunshine duration. Comparing these maps, the median cloud cover appears to be significantly higher than its corresponding mean, with exceptions for the Mediterranean Sea, Portugal, and areas south of Spain and Italy. For areas where the median exceeds the mean, it means that periods of very low cloud cover occur only infrequently. This is consistent with the results of strong but infrequent solar irradiations over Europe (see Section 3.1).

Other areas noted in Section 3.2 are also discernable: areas from south of France to south of Spain have strong solar potential, with a mean cloud cover below 50%. **Figure 8c** presents the variance of the hourly cloud cover, averaged over 31 years, over the sunshine duration. Areas of low mean cloud cover (Figure 8a) generally show greater variance. These areas south of Europe also have a very low median cloud cover (below 0.3); this increased variance could be explained by heavy but infrequent cloud cover.

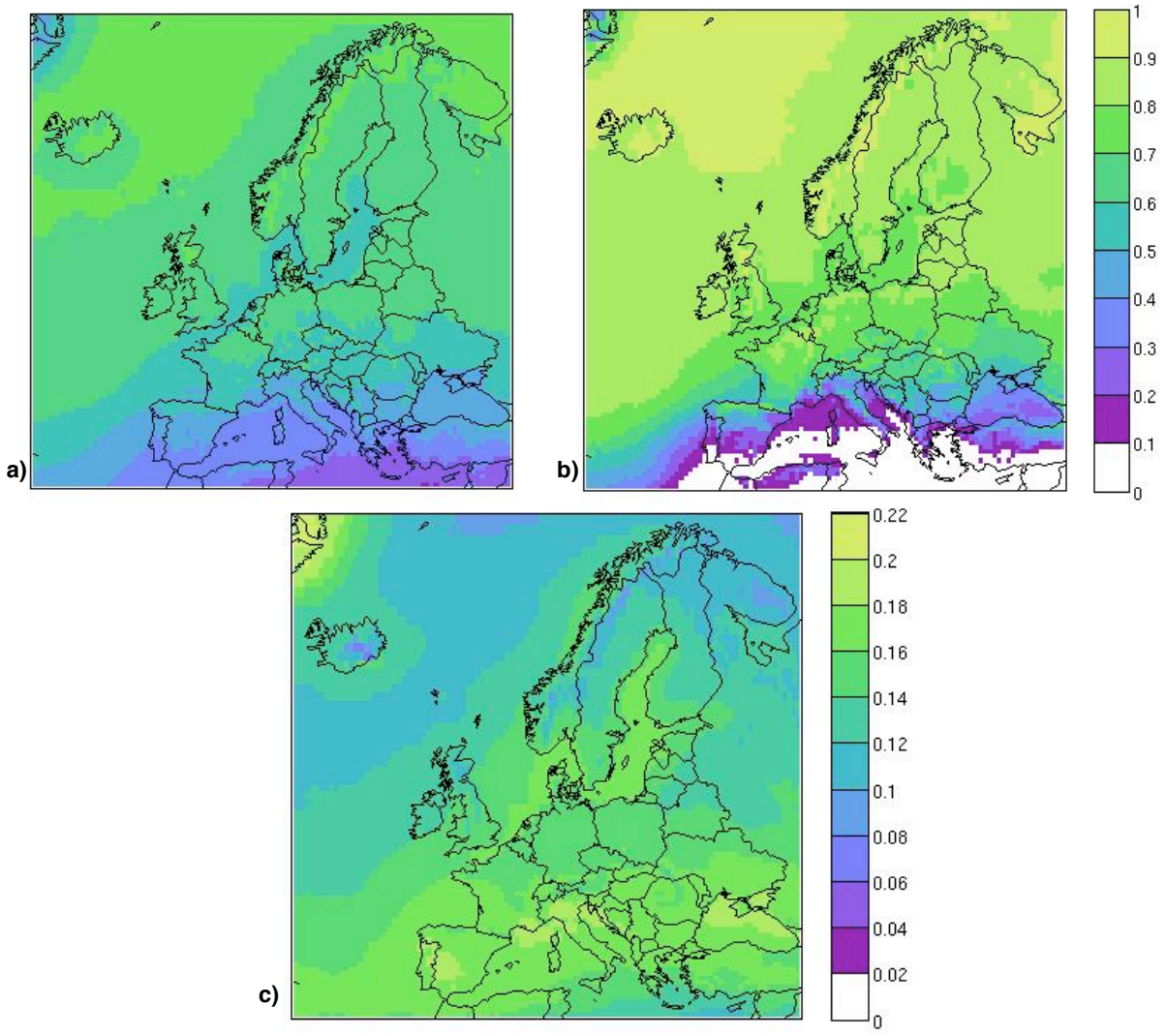

Figure 8. Geographical variation of the mean (a), median (b) and hourly (c) cloud cover fraction (unitless), averaged over the sunshine duration.

3.4 Comparative Study

In order to validate our cloud cover results, we have chosen to compare the MERRA data with cloud cover estimates from other satellites. Data from the Satellite Application Facility on Climate Monitoring (CM SAF) has been used. This data results from processing the first-generation Meteosat satellite record (Posselt *et al.*, 2012; Mueller *et al.,* 2012). CM SAF cloud products are derived from NOAA and METEOSAT satellites. The CM SAF algorithm is

based on a multi-spectral threshold technique: for every satellite, the threshold technique is applied to every pixel of the satellite image that could be visible, infrared, passive or active microwave.[1] CM SAF has a finer spatial resolution than the MERRA data—¼° (lat) × ¼° (lon)—and is available as daily means spanning 14 years (from January 1996 to December 2009).

The mean cloud cover based on these years computed with the CM SAF and MERRA data are displayed respectively on **Figures 9a and 9b**. The features of the two maps are quite similar, with mean cloud cover generally about 0.1 higher for CM SAF. For both maps, we find low mean cloud cover (<0.5) in southern Europe, medium mean cloud cover (0.5–0.7) in central and northern Europe, and strong mean cloud cover (>0.7) over the ocean. One pattern observed with MERRA data, which is not apparent with CM SAF, is the reduced cloud cover over the North Sea and the Baltic Sea. The largest contrast is observed over the ocean, where the CM SAF mean is systematically 0.1 higher than MERRA.

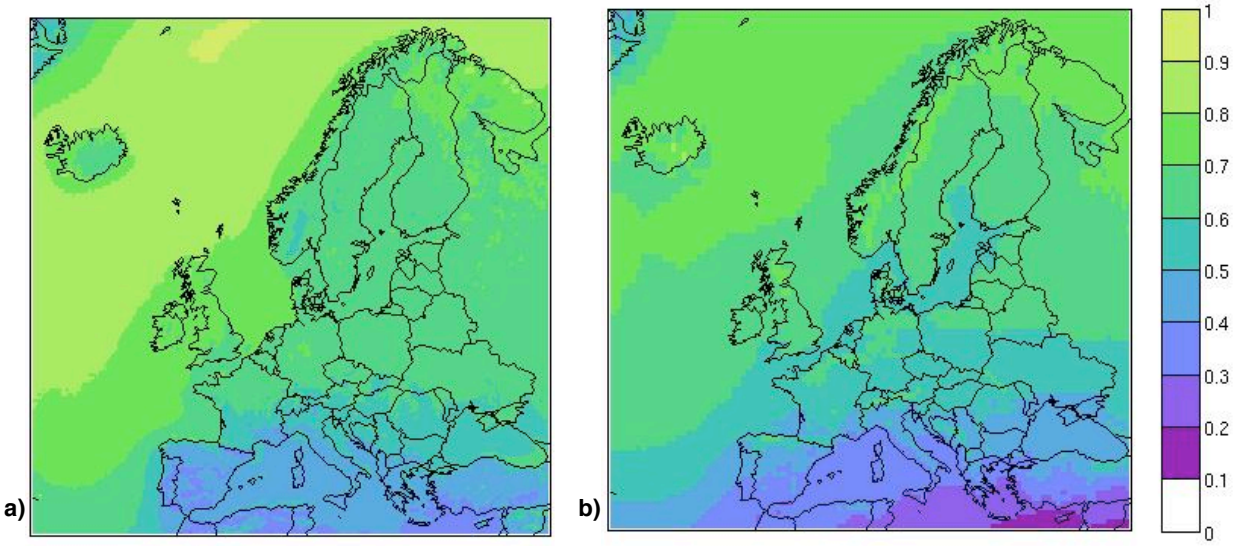

Figure 9. Geographical variation of the mean cloud cover fraction (unitless) based on the years 1996 to 2009, computed with the CM SAF data (a) and MERRA data (b).

The median cloud cover, based on the same years and computed from CM SAF and MERRA data, respectively, are also shown on **Figures 10a and 10b**. For both data sets the median values are higher than the mean values above the ocean, central Europe and northern Europe. However, for Spain, Portugal, Italy and the Mediterranean Sea, the median and mean values seem to be very consistent between both data sets (except for MERRA, south of the Mediterranean Sea, where the median is slightly below the mean). Differences between the means appear similarly between the medians: CM SAF values are higher than MERRA values by about 0.1, primarily over the ocean. We display the variance of the daily fractional cloud cover computed from CM SAF and MERRA data on **Figure 11**. The CM SAF data show greater variance than

[1] More details about the CM SAF algorithm are available online on the CM SAF website (http://www.cmsaf.eu/EU/Home/home_node.html).

MERRA over most of the mainland Europe, above the Mediterranean, the North Sea and the Baltic Sea, whereas it is the contrary above the ocean.

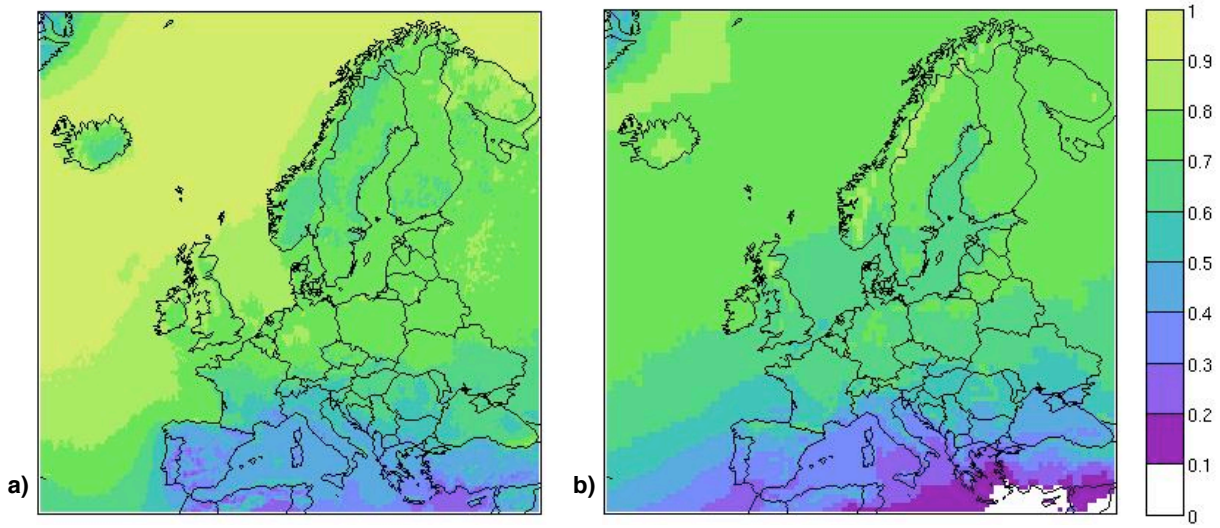

Figure 10. Geographical variation of the median cloud cover fraction (unitless) based on the years 1996 to 2009, computed with the CM SAF data (a) and MERRA data (b).

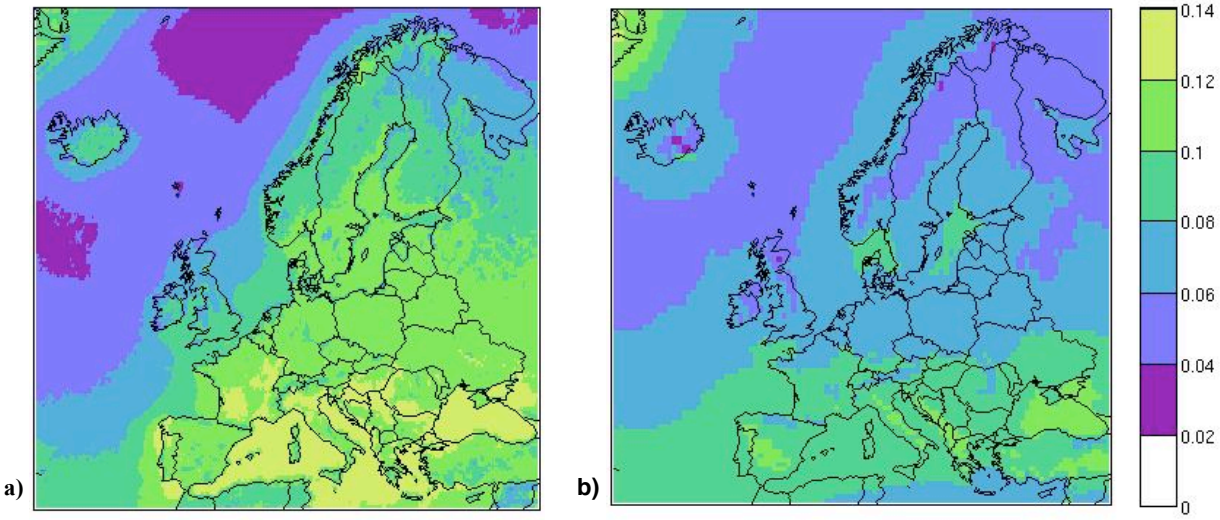

Figure 11. Geographical variation of the variance of cloud cover fraction (unitless) based on the years 1996 to 2009, computed from CM SAF data (a) and MERRA data (b).

To finally understand how close and compatible these two datasets are, a correlation study has been carried out. For every point of the grid, the pair of values from CM SAF and MERRA is extracted. Then we calculate for every pair (*x,y*) the correlation coefficient *Rho*, defined as:

$$Rho = \frac{Cov(x,y)}{\sigma_x \, \sigma_y} \tag{6}$$

where *Cov* stands for the covariance and σ for the standard deviation. *Rho* values range between -1 and +1, where 1 is a total positive correlation, 0 is no correlation and -1 is a total negative correlation (also called total anti-correlation).

The first correlation study has been done on the daily means of cloud cover (CM SAF data is only available as daily means) and is displayed in **Figure 12a** (areas shaded for correlations at the 5% significance level). Two main areas are discernable. The first includes the Atlantic Ocean, Iceland, Ireland, the United Kingdom and northeast Scandinavian countries, and shows either slight negative correlation or non-significant correlation values at the 5% significance level. The second area includes the remainder of mainland Europe and the Mediterranean Sea, and the majority of this region contains significant positive correlation, with a maximum of 0.4. These low positive and slight negative correlations could have been expected given the inherent chaotic nature of cloudiness, particularly at daily timescales, and the limits of predictability implied by the strongly non-linear processes that govern cloud formation. Moreover, the calculation of CM SAF products induces a higher variability than MERRA over ocean surfaces (+10–15%—see Figure 11), which could explain the lack of confidence in correlation above the Atlantic Ocean. There could also be a bias in the calibration of the CM SAF, due to a lack of ground measurements in the Atlantic Ocean.

The second correlation study (**Figure 12b**) has been carried out on a monthly basis. Spatial features found in the daily results are also seen here: slight negative correlation over Iceland, Scotland and the northeast of the Scandinavian countries, with insignificant correlation (below the 5% level) elsewhere. The remaining area shows positive correlations from 0.4 to 0.9—stronger than in the daily results. Perhaps more importantly, the regions also contain among the strongest solar resource potential (see Figures 1–3). This area is therefore of considerable interest to our overall analyses of resource potential and to providing a credible assessment.

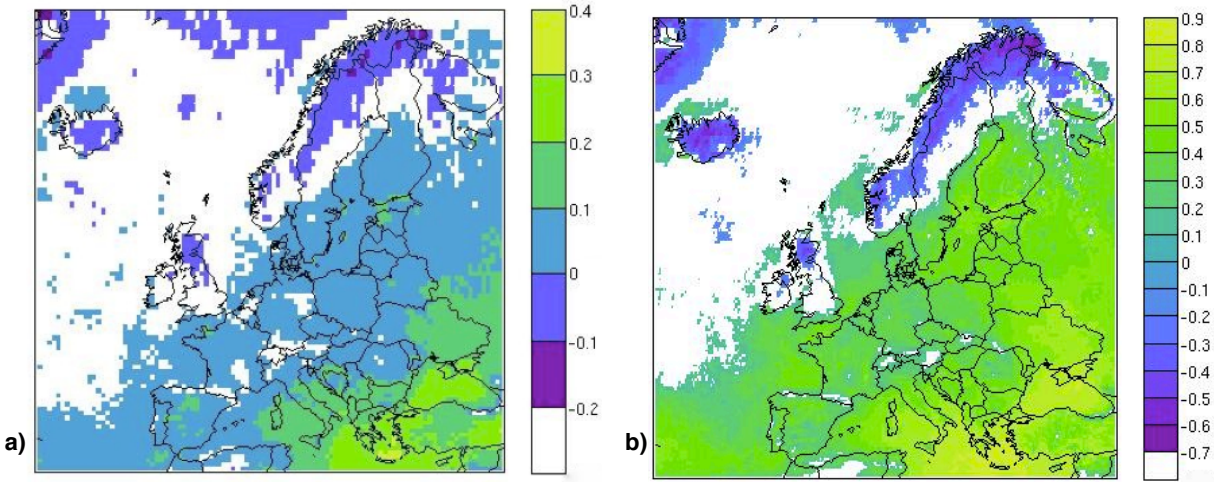

Figure 12. Geographical variation of the correlation coefficient of CM SAF and MERRA daily (a) and monthly (b) data sets, based on the years 1996 to 2009. Areas are only shaded for correlation values at a significance level of 5%.

4. ASSESSMENT OF SOLAR POWER RESOURCE

4.1 Availability of Solar Power

We observed that median solar irradiation was quite lower than its mean. If an area's mean is above the cut-off value, a majority of its values over the entire timespan may still be below, and we can further quantify the overall availability of solar resource. The availability of solar power can be defined as:

$$Availability = \frac{\#\ of\ hours\ with\ solar\ power \geq cut-off}{Total\ \#\ of\ hours} \tag{7}$$

For this study, we have chosen cut-off values based on the thresholds indicated by Ubertini and Desideri (2002), which range between 20 and 80 W/m^2, presumably depending on technological aspects of the PV cells. To assess the sensitivity of this cut-off range on our availability metric, **Figures 13a, 13b and 13c** show the dimensionless availability of solar power useable for PV based on 31 years (averaged over the sunshine duration) for three cut-off values of 80, 40 and 20 W/m^2, respectively.

Once again, the result shown in Figure 13a (cut-off of 80 W/m^2) is consistent with the observation of two areas in Europe: southern Europe (for latitudes south of France) displays an availability factor above 0.5, meaning that for more than 50% of each day (from sunrise to sunset) solar power is harvestable. On the contrary, areas north of France show availability factors below 0.5, which means that more than half of the time solar power is not available. Figures 13b and 13c show that availability increases with better technology and lower thresholds: a cut-off value of 40 W/m^2 would be sufficient to provide all of Europe with an availability factor above 0.5; A cut-off value of 20 W/m^2 would provide most of Europe with an availability factor above 0.7. This increase could be primarily attributed to diffuse solar irradiation, as it is always available during daytime, and is not often below 20 W/m^2 (see Figure 3).

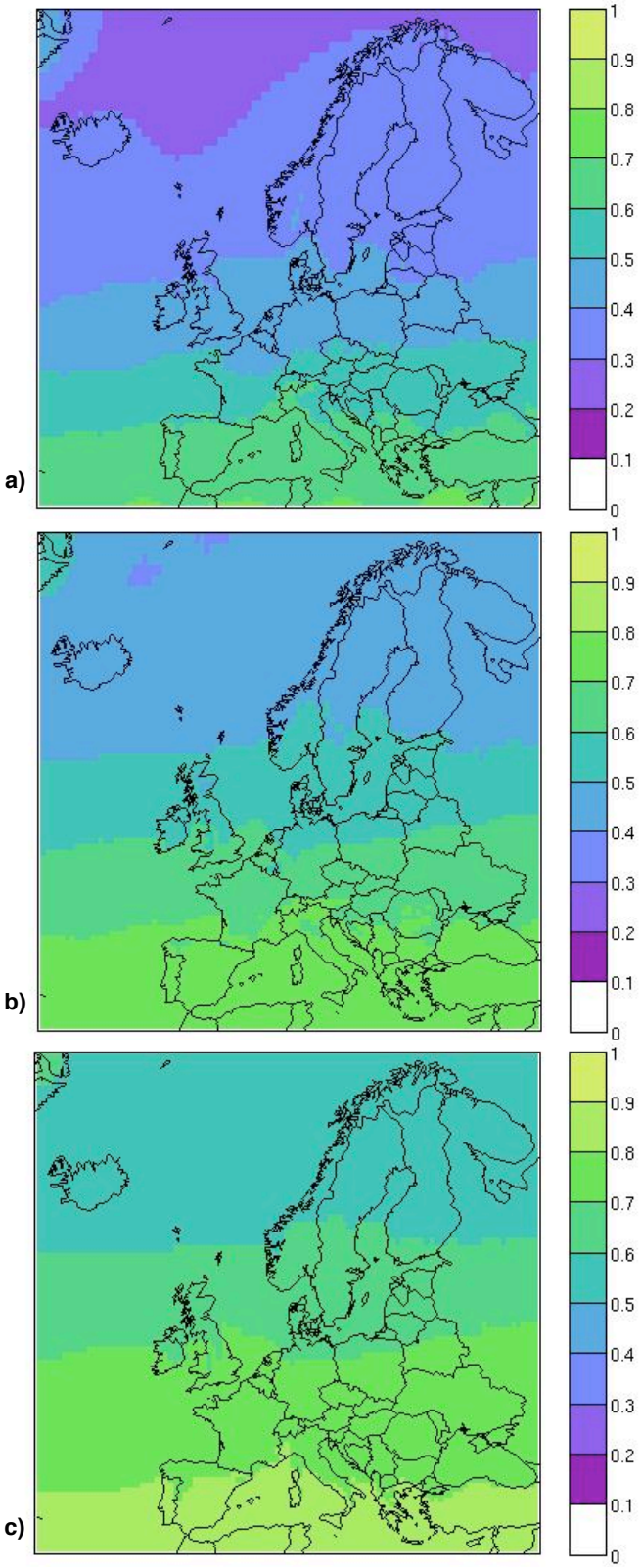

Figure 13. Geographical variation of dimensionless availability of solar power useable for PV, with cut-off values of 80 W/m^2 (a), 40 W/m^2 (b) and 20 W/m^2 (c).

4.2 Distinction Between Variability and Intermittency

As described in Cosseron *et al.* (2014), intermittency and variability are both used to characterize renewable power. Solar power intermittency will refer to the switch between a solar power generation state (when solar power is above the cut-off) and a no power generation state (when solar power is below the cut-off value and is therefore not harvestable). On the other hand, variability only refers to states with solar power generation (when solar power is above the cut-off value) and quantifies the variations over time of solar power when harvestable.

Figure 14 illustrates those two different types of fluctuations. It shows the total solar power useable for PV at a location in central Europe during 200 consecutive hours of February 1979. The black line represents the cut-off value of 80 W/m^2. When solar power is above this threshold, it varies, showing some peaks, and this is what we call the variability (for example, between the 82nd and the 90th hours). Conversely, the solar power often decreases to values below 80 W/m^2 (around the 18th hour, for example). This is what we distinguish as intermittency.

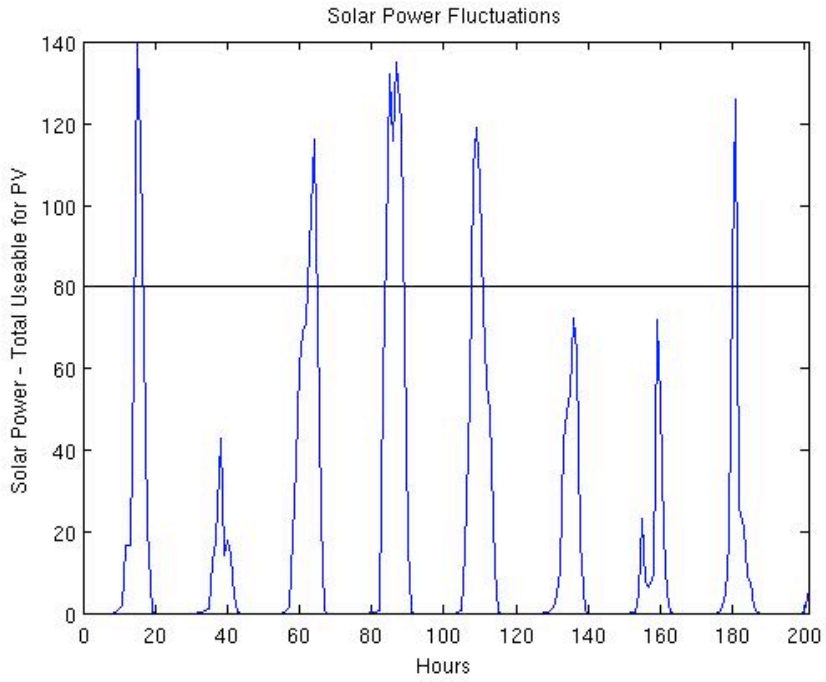

Figure 14. Illustrative solar power irradiation (W/m^2) showing fluctuations.

4.3 Spatial Coincidence of Intermittency

Our results have shown so far that for every location, both variability and intermittency are experienced regularly, and that availability coefficients are never equal to 1. Since we aim to have power available at all times, intermittency is more harmful than variability. As our ultimate aim is to mitigate intermittency by aggregating spatially dispersed PV panels, we study the spatial variation of intermittency since intermittency varies from one location to another. To effectively reduce the intermittency, solar power must be present and harvestable in at least one of two (or more) connected sites, assuming a cut-off value of 80 W/m^2. In that respect, our time

data set (only over the sunshine duration) for every point of the grid is converted into a binary sequence of 1s and 0s, illustrating if solar power is harvestable or not. Each point is then compared to its closest neighbors in a box of 19 × 19 grid points, which represents nine points in each direction. This box stands with the MERRA data as an approximately 1000 km × 1000 km domain, centered on the grid point of interest. The process, as explained by Gunturu and Schlosser (2011), is illustrated by **Figure 15**. If the center of the box is called *R,* and *P* is one of *R*'s nine closest neighbors in each direction, we compare for every point of the time series with covariation of those two points. Then, depending on the criterion chosen, the score of the point *R* will be the number of points *P* that fulfill this criterion. In order to cover the entire grid, the center of the box *R* is changed and the score determined.

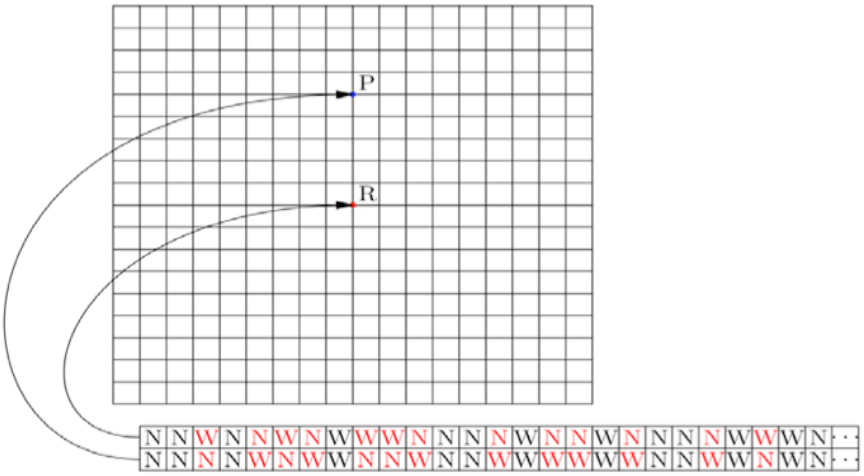

Figure 15. Schematic illustrating the intermittency study, from Gunturu and Schlosser (2011, Figure 19).

4.3.1 First Criterion: antiCoincidence

Following the work done by Cosseron *et al.* (2014) on the wind power over Europe, the criterion of *antiCoincidence* has been studied. For this first metric, the hours when one of the two points *R* or *P* (but not both) has solar power greater than 80 W/m^2 are counted. The total count is then compared to the complete time series (for the sunshine duration). If more than 50% of the time, one of the points shows harvestable solar power when the other one does not, then the criterion is fulfilled and the two points are said to be antiCoincident. The total score for every point of the grid is the number of antiCoincident points around them, normalized by the total number of points in the box of approximately 1000 km^2. The 50% limit was chosen for the wind study, but was not suitable for the study of solar power: no antiCoincident pair was found. Relaxing the criterion to 25% didn't lead to any further expanse of regions containing antiCoincidence.

4.3.2 Second Criterion: antiNullCoincidence

Although there was no widespread evidence of antiCoincidence for solar power, an additional metric has also been studied: the *antiNullCoincidence*. We count now the hours when *P* has solar power above the threshold and when *R* has no power harvestable. Then the count is compared

with the total number of hours (only during the sunshine duration) when *R* has no solar power. If R has no power harvestable while P has usable solar power at least 50% of the time, then the criterion is fulfilled and the two points are said to be antiNullCoincident. Once again, we used a 50% limit as in the Cosseron *et al.* (2014) wind study, but—similar to the antiCoincidence results—there were no widespread regions of antiNullCoincident pairs. By relaxing the criteria to 25%, the results show some modest occurrence of this trait (**Figure 16**). Blank areas show absence of significant antiNullCoincidence. Non-zero values never surpass 0.5 and are highest over France, Spain, Italy, Germany, Greece and the Adriatic countries, as well as offshore from France and Portugal. These regions indicate some modest gains would be possible from interconnecting solar farms to provide a steadier aggregate solar power supply.

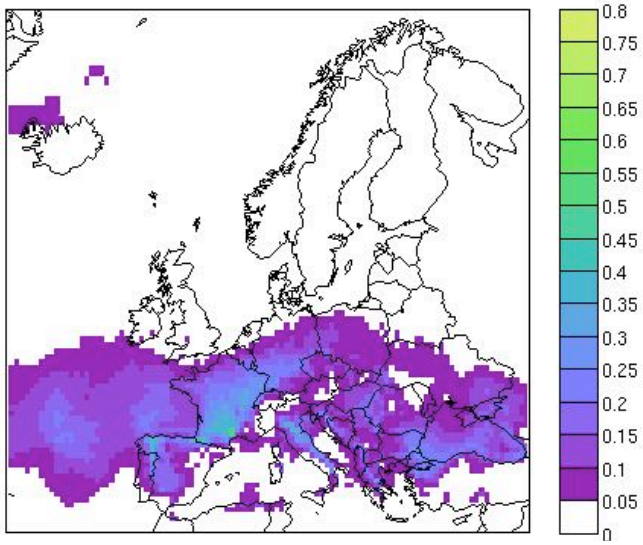

Figure 16. Geographical variation of the normalized antiNullCoincidence parameter for solar power over Europe, over the sunshine duration.

We consider this metric further by computing the antiNullCoincidence parameter during both the cold and the warm seasons. The results are displayed in **Figure 17**. Note that the map for the cold season is similar to the map for all seasons. AntiNullCoincidence is quite scarce during the cold season, but because the criterion must be fulfilled only 25% of the time, antiNullCoincidence does not appear to be more common over all seasons. However, during the warm season, results show non-zero antiNullCoincidence over almost the whole continent and the ocean. One explanation for this difference is that the highest latitudes do not benefit as much from solar potential; as we noticed in Figure 2a, latitudes higher than south of France have a mean solar irradiation below the threshold of 80 W/m^2, indicating that harvestable solar power may be scarce in these regions. Thus, in such locations, it is difficult to fulfill the antiNullCoincident criterion during the cold season. During the warm season, Figure 2b indicates mean solar power harvestable everywhere, which enable the criterion antiNullCoincident to be more likely. One section of both of these maps still needs further clarification: southern Europe and the Mediterranean Sea do not show sufficient antiNullCoincidence during both seasons. This

could be because solar potential is high in these areas, leading to few situations where one location has power and another does not.

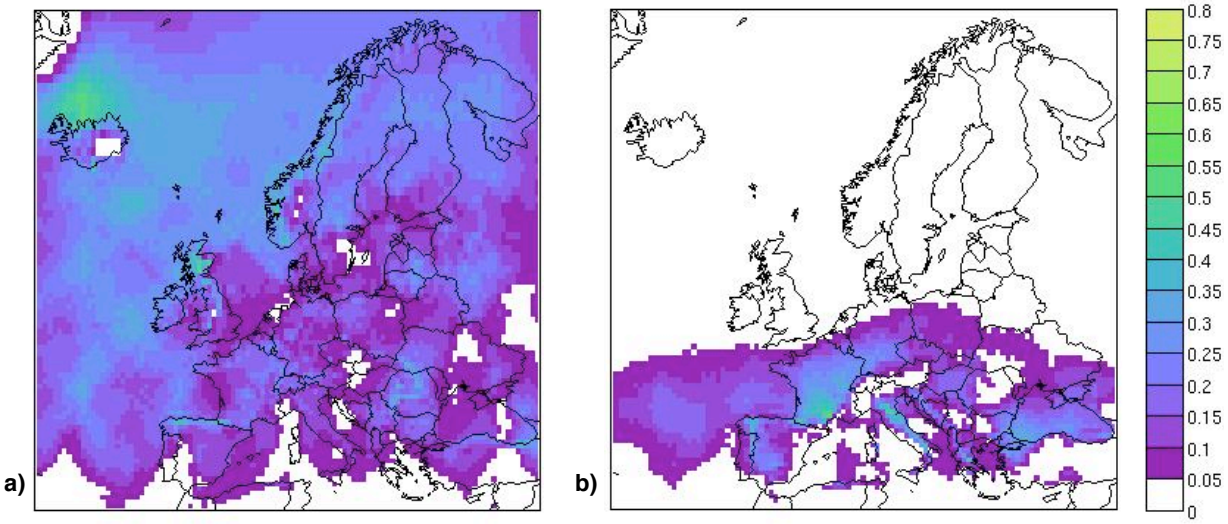

Figure 17. Geographical variation of the normalized antiNullCoincidence parameter for solar power during the cold season (a) and the warm season (b), over the sunshine duration.

5. BENEFITS OF CO-LOCATION OF SOLAR AND WIND POWER INSTALLATIONS

In this section, the wind data sets used are the same as Cosseron *et al.* (2014) and are computed from MERRA data, with the same time span, spatial resolution and time resolution as our solar data. In line with this previous study, we have considered here the wind power density (WPD) for a turbine height of 80 m, which is most common in terms of the current deployment of this generation technology.

For the analysis presented in this section, we envision a (hypothetical) deployment landscape where solar and wind generation is "co-located" within every grid point. For this assessment of co-located generation technologies, we recalculate the aforementioned availability and intermittency metrics while combining previously constructed individual solar and wind resource estimates for each grid point. As such, we do not consider any interactions that might occur between the solar and wind farms and their surrounding environment (i.e. weather/climate effects) or how these may affect their individual and subsequent aggregate resource availability, as this would require highly-resolved observations and a modeling effort that is not only outside the scope of this analysis, but also a formidable research task given current state-of-the-art models.

5.1 Availability of Solar and Wind Power

A first criterion to evaluate the benefits of co-location would be the change in availability of this combined renewable power generation. We have shown in Section 4.1 that the availability of solar power depends mainly on latitude, and that with a threshold of 80 W/m^2, power availability was below 50% (a dimensionless coefficient below 0.5) for all the latitudes north of France. Cosseron *et al.* (2014) have shown that the availability of wind power with a threshold of 200 W/m^2 was above 0.5 only in Ireland, in the United Kingdom and offshore. Values between

0.4 and 0.5 were also noticeable on the English Channel, North Sea and Baltic Sea coasts. **Figure 18** shows the dimensionless availability of wind power density as computed by Cosseron *et al.* (2014) (threshold of 200 W/m^2, averaged over 31 years) compared alongside the corresponding availability estimates of solar power with a cut-off of 80 W/m^2. We consider only daylight hours for solar power availability, as the aim of this metric is to quantify the portion of power generation that is available during periods when it is known to potentially exist (i.e. night-time hours have no potential for solar power). For comparison, wind power availability is also computed only from sunrise to sunset. As such, availability of solar power over land generally appears more extensive than that of wind. Over ocean points, wind shows greater availability at higher latitudes, while solar is dominant at lower latitudes for our domain of interest. However, when making these generalizations, it is important to note that the prescribed threshold values for cut-off in generation are also quite different between these technologies; therefore, although PV systems can produce electricity with only 80 W/m^2, the generated amount of electricity will be lower than when wind production crosses its threshold at 200 W/m^2 wind power density. As previously noted, the values of these cut-offs were prescribed to reflect the most widespread technology that is currently deployed among the larger wind and solar farms. As such, if the size of wind turbines (i.e. installed capacity) were reduced, so would be their cut-off values, and thus we might expect wind availability to improve in many areas—perhaps becoming comparable to solar. Likewise, improvements in PV technology would presumably have benefits to the solar cut-off values considered here.

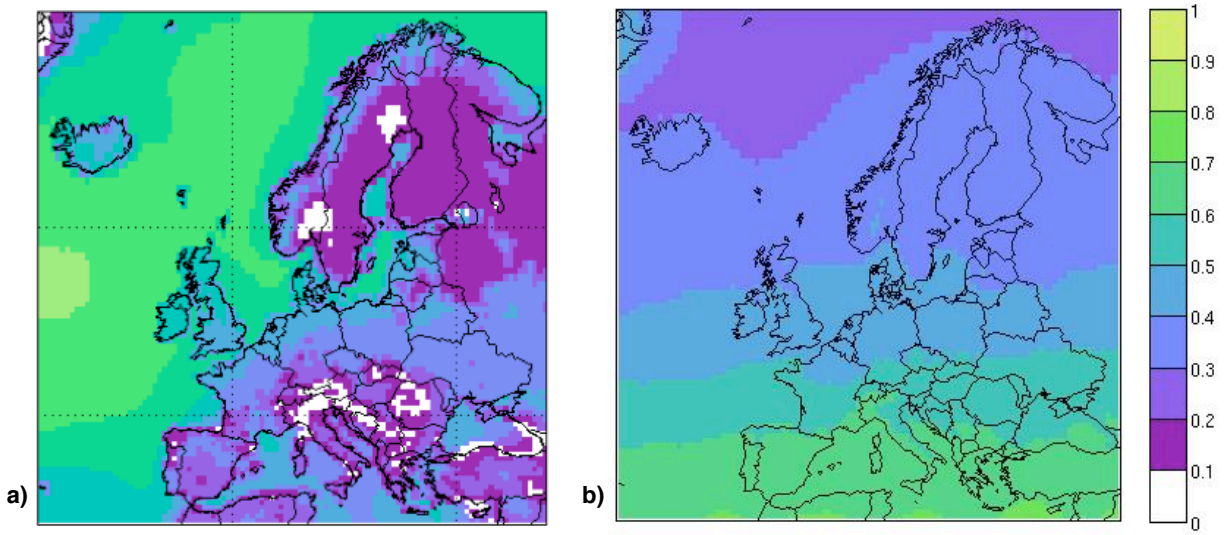

Figure 18. Geographical variation of the dimensionless availability of wind power at 80 m (a) and of solar power (b). The calculation was made only during the sunshine duration.

To further assess the co-location of solar and wind power, we have computed the availability of both powers as the number of hours where wind, solar, or both are above their threshold value, divided by the total number of hours. As above, the cut-off values used are 80 W/m^2 for solar and 200 W/m^2 for wind. **Figure 19** displays this dimensionless availability of the combined solar and wind power generation, from sunrise to sunset. Note that no areas are left with availability below

0.3. The Scandinavian countries benefit least from co-location. The zones showing the greatest availability are Spain, Portugal and south of France, where solar availability is strong, and offshore locations, Ireland, the United Kingdom, the English Channel, the North Sea and Baltic Sea Coasts where wind availability is strong. Except for southern Europe, where solar seems to dominate, the fingerprint of wind power availability can be seen in a general sense by the land-sea contrast (more specifically, by the zones of low availability in Sweden, Norway and Finland), as well as relatively moderate availability in central Europe (even if the values are higher as a result of co-located solar power).

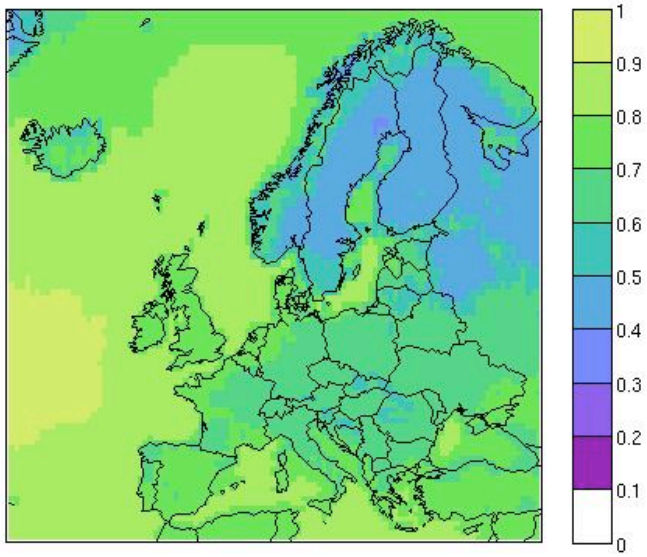

Figure 19. Geographical variation of the dimensionless availability of solar and wind power co-location, averaged over the sunshine duration.

In order to assess availability over full 24-hour days and not only over sunshine duration, we have considered the availability of wind power at night, with a threshold of 200 W/m^2 (see **Figure 20**). The result is comparable to Cosseron *et al.* (2014), with the same zone of relatively strong availability over oceans. In a co-located system of wind and solar power generation, the availability of power will be limited to wind at night (i.e. Figure 20). Thus, the results of Figures 19 and 20 indicate that for many land regions over our domain of interest, under current technologies, there will remain considerable diurnal fluctuations in the availability of power generation from co-located solar and wind farms.

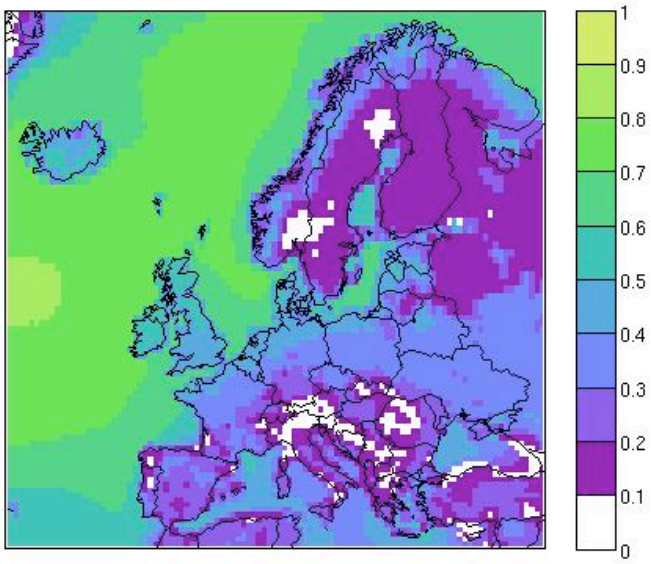

Figure 20. Geographical variation of dimensionless availability of wind power at night.

5.2 Correlation Study

A primary benefit of the co-location of wind and solar resources is that one source could harvest power when the other is not harvestable. In a system where every point could benefit from either wind or solar power, the availability of power increases; however, that only captures instances where either or both resources are available, and is not able to quantify the variability of these resources. According to Heide *et al.* (2010), the seasonal solar power generation should anti-correlate with seasonal wind generation. To complement our understanding of how solar and wind power effectively counterbalance each other, a correlation study between those two resources has been carried out. Correlation coefficients and *P*-values, as defined in Section 3.5, have been estimated at four different time scales: seasonally, monthly, daily and hourly. Areas with *P*-values above 0.05 have been left blank in order to highlight the areas (shaded) at the 5% significance level. The correlation study has been done with Pearson and Spearman's methods, and both results were qualitatively equivalent. Thus, for the sake of brevity, we present the results obtained with Pearson's method.

As expected, seasonal behavior shows negative correlation between wind and solar potentials, since wind tends to be stronger in winter months (during stronger baroclinity of the atmosphere and associated synoptic-scale weather systems) when the solar potential is low. However, the strongest winds are not always harvestable, as they could damage a windmill. Such high wind speeds, if not harvestable, would count as a zero value and therefore correlate with low solar potential during the winter. In that respect we have counted the total amount of cut-out occurrence for wind power (the cut-out is the highest operable wind speed of widespread technologies that are deployed—powers above the cut-out are not harvestable and therefore register as a zero value). According to Kriesche and Schlosser (2014) power curves, the cut-out chosen for wind speeds is 25 m/s. Over 31 years of hourly data, the total number of cut-out occurrence over the ocean represents less than 1% of the total time series. We will therefore

consider the wind cut-out as non-significant in this study. **Figure 21a** shows the correlation coefficient of seasonal means between wind and solar powers. Areas of positive correlation over our domain of interest are quite limited (e.g. Portugal and Turkey). The anti-correlation is seasonally strong and is very high above the ocean, Iceland, Ireland and the United Kingdom. The remaining lands of Europe still show strong negative correlation (between -1 and -0.4).

The correlation results computed between monthly means are illustrated on **Figure 21b**. Once again, the Atlantic Ocean shows strong and uniform negative correlation while the main inland areas still shows negative but more textured correlation. Compared to the correlations resulting from seasonal means, the anti-correlation values are lower for monthly means, and the regions of insignificant or positive correlation in Portugal and Turkey are consistent.

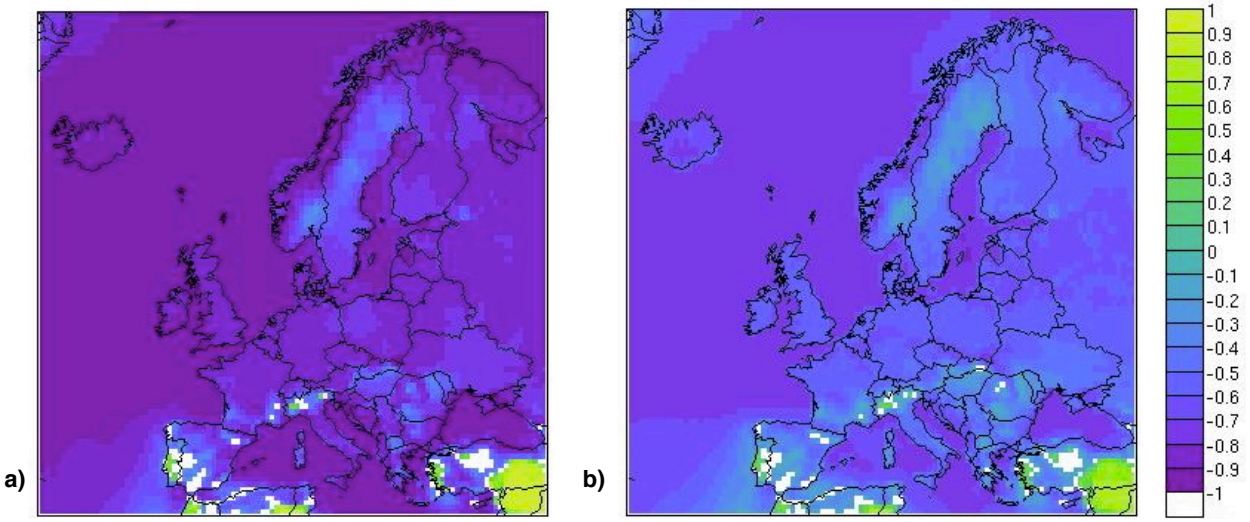

Figure 21. Geographical variation of the correlation coefficient of seasonal (a) and monthly (b) means between wind and solar powers. Shaded values indicate correlations at a significance level of 5%.

On **Figure 22**, we display the correlation coefficient between wind and solar powers for daily and hourly means. As we become more resolved in the time scale, we find fewer areas with significant strong negative correlation. Nevertheless, the patterns from monthly and seasonal results are largely maintained for the daily correlations, with the strongest negative correlation above the ocean, and with positive correlation appearing over southern Europe. At an hourly scale, both negative and positive values are low (most of them between -0.2 and 0.2); however, they are still significant. We also see that the aforementioned areas of non-significant correlation in southern Europe have been diminished, and in most cases, substituted with positive correlation. However some non-significant regions appear in Ireland, Scotland and the Scandinavian countries. At the hourly timescale, the majority of land now displays slight positive correlation, likely due to the sun warming the ground during the day, stirring up the wind which peaks in speed during the afternoon.

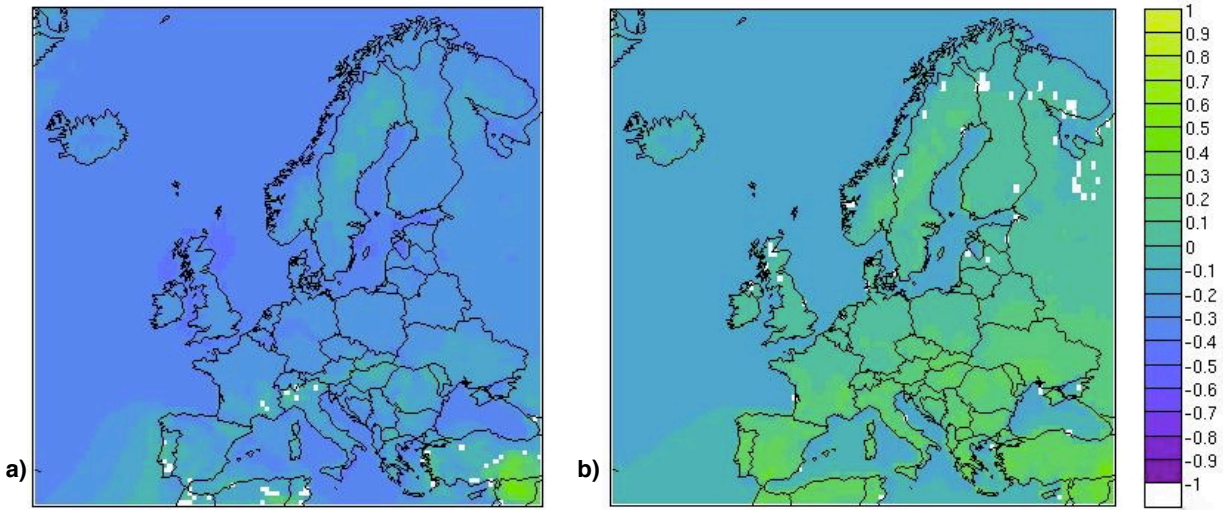

Figure 22. Geographical variation of the correlation coefficient of daily (a) and hourly (b) means between wind and solar powers. Shaded values indicate correlations at a significance level of 5%.

5.3 Peak-to-Trough Mitigation

As previously shown, the strong seasonal and monthly anti-correlation between solar and wind power could have strong impacts on the aggregate electricity generation. If the maximum solar radiation peak and minimum wind power density peak occurs approximately at the same time, concurrently followed by the minimum solar peak and maximum wind peak occurring at nearly the same time, the peak-to-trough difference (maximum to minimum difference) of the aggregate power could be lower than the peak-to-trough of one isolated power resource, as each minimum offsets the other maximum. This implies that aggregating those resources could result in steadier electricity generation, and potentially less impact from peak-to-trough power differences from local co-located generation sources to aggregate operations and power dispatch.

In order to assess peak-to-trough mitigation possible through aggregation of powers, we have first computed the monthly mean wind power density with its peak-to-trough difference for every grid point. Then, the monthly means of aggregated solar radiation and wind power density (taking into account cut-off and cut-out values) have been calculated to assess the peak-to-trough difference of the total power for every grid point. Finally the difference (wind-only minus wind-and-solar) between the two peak-to-trough values is displayed on **Figure 23**.

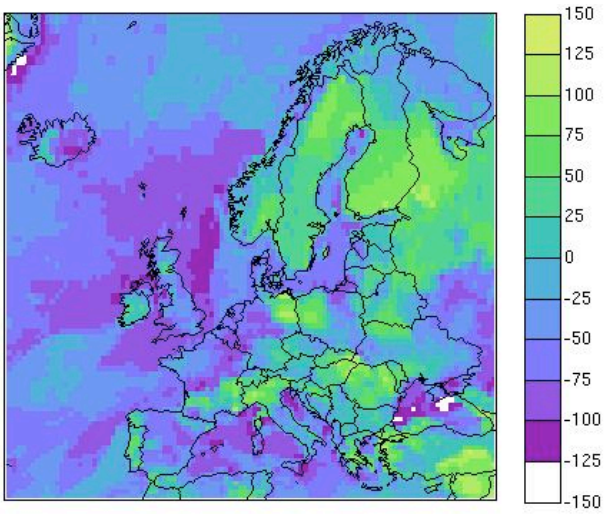

Figure 23. Geographical variation of the difference in peak-to-trough of monthly power density over Europe. The difference is calculated as the value from wind power alone minus the value that results from the combined wind and solar resource. Results are in units of W/m^2.

Contrary to our expectations, there are many areas where the peak-to-trough difference increased. This is the case for a majority of inland locations, especially in central Europe and in the Scandinavian and Baltic regions. Above the ocean, the Mediterranean Sea, Spain and coastal region of the North Sea, the peak-to-trough shows a decrease.

The increase in the peak-to-trough difference observed in central Europe and in the Scandinavian and Baltic regions, instead of an offset, is likely due to the lack of wind power density in these areas. Indeed, looking at Figure 18, it appears that in these regions the wind power density availability is very low, meaning that most of the time the wind power is below the cut-off value (thus equal to zero in our calculation). In that case, the mean peak-to-trough difference for the wind, usually very high, is on the contrary very low and could be increased by strong solar potential occurring in summer months.

5.4 Mitigation of Intermittency

The goal of this section is to effectively mitigate intermittency through aggregation of two renewable powers that have shown anti-correlation at seasonal and monthly timescales. As seen in Section 5.1, aggregating wind and solar powers results in an increase of power availability. Still, co-location of wind and solar power does not reach an availability coefficient of 100%, and some intermittency is expected. Nevertheless, we know that interconnections of dispersed wind turbines could result in mitigation of wind power intermittency, and that interconnecting PV panels could have a similar impact on solar power intermittency. In this regard, we consider the geophysical aggregation of dispersed wind turbines and dispersed PV panels: to effectively reduce intermittency, wind or solar power must be present in at least one of two (or more) connected locations.

We show on **Figure 24** the antiNullCoincidence parameter (as described in Section 4.3.2) computed for the co-location of solar and wind resources during the sunshine duration. As a

comparison, we display in **Figure 25** the antiNullCoincidence parameter for wind power density alone (Figure 25a) and for solar power alone (Figure 25b), computed during the sunshine duration. Once again, the wind power seems to impose its pattern to the co-location: all the areas where antiNullCoincidence was found for wind are also displaying antiNullCoincidence for the co-location. Looking at these areas in detail, we find that the antiNullCoincidence coefficients are increased due to the co-location of wind and solar power generation, reaching the greatest values above the Atlantic Ocean, Iceland, Ireland, Scotland and Portugal. Besides the areas where antiNullCoincidence was already significant with only wind, we identify new inland locations showing antiNullCoincidence due to co-location: the Baltic countries, Poland, most of France, Spain, Italy, Greece and Turkey. Note that the areas showing antiNullCoincidence are almost only offshore locations or coastal countries.

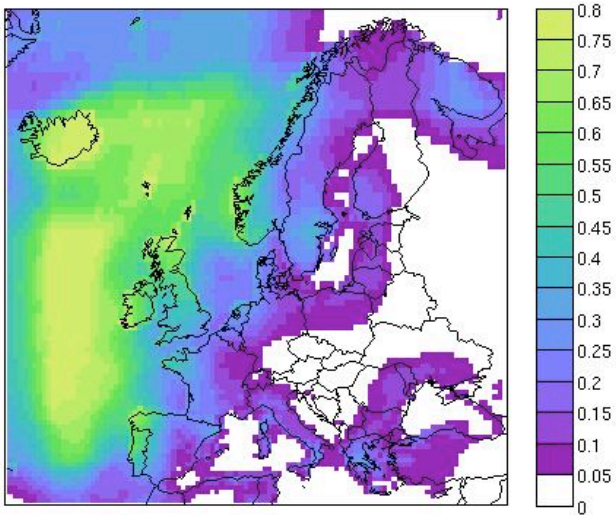

Figure 24. Geographical variation of the normalized antiNullCoincidence parameter for the co-location of wind and solar powers, over the sunshine duration.

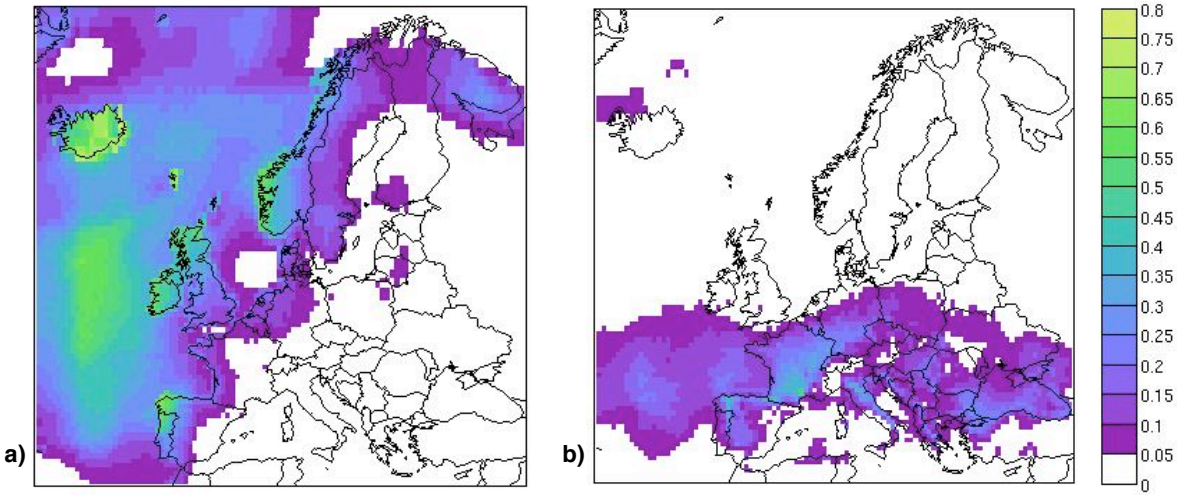

Figure 25. Geographical variation of the normalized antiNullCoincidence parameter for wind power density at 80 m (a, stricter criterion) and solar power (b, relaxed criterion), over the sunshine duration.

The areas of greatest benefit to co-location, in terms of mitigation of intermittency, are the Mediterranean coastal countries and the Baltic regions. The Mediterranean countries show a lack of antiNullCoincidence for wind, and some antiNullCoincidence for solar (albeit with a relaxed criterion—see Section 4.3.2) but their co-location results in a significant antiNullCoincidence (using the stricter criterion as described in Section 4.3.2). This benefit is even more striking for the Baltic regions where significant antiNullCoincidence does not result from solar or wind alone, but appears with co-location. However, the result for the Baltic regions should be put in perspective: indeed, in this area solar power is usually low and the total amount of power delivered to the grid is not as high as it would be for the Mediterranean countries (which have a higher solar power resource); therefore, Baltic regions would benefit more from co-location and antiNullCoincidence.

We have plotted on **Figure 26** the antiNullCoincidence parameter for wind only during the night for a more comprehensive assessment of the possible mitigation of intermittency. Both maps of antiNullCoincidence during daytime and nighttime are very similar, meaning that the diurnal cycle has very little impact on our parameters. During the night, only the coastal Atlantic regions with onshore locations would benefit from antiNullCoincidence—similar to the study over the United States conducted by Gunturu and Schlosser (2011). We find high antiNullCoincidence in Iceland, Ireland, Scotland, Finland and Northwestern Portugal and Spain, with the highest values reaching 0.7 or even 0.8 with only wind at night, whereas the highest values of only solar during the day are around 0.5 (Figure 25).

These coastal regions could therefore mitigate the intermittency of solar and wind resources by co-location during the day, and by interconnecting wind farms at night. Some regions benefiting from co-location during the day, such as the Mediterranean coast and the Baltic regions, would need other intermittency mitigation at night, such as storage or backup technologies.

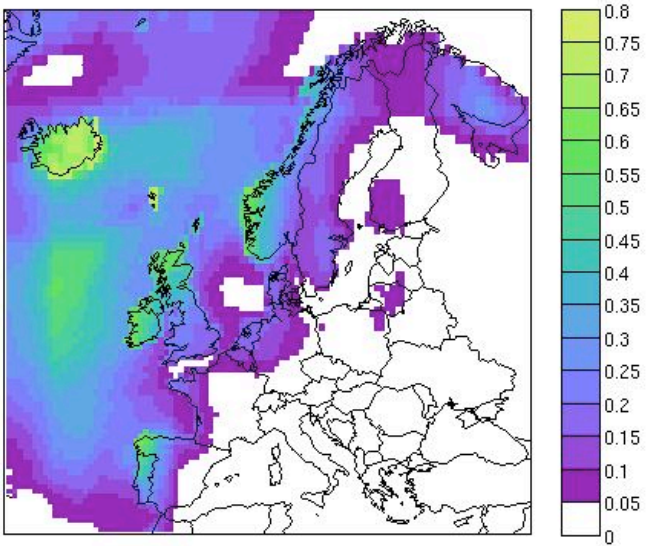

Figure 26. Geographical variation of the antiNullCoincidence parameter for wind power as described by Cosseron *et al.* (2014)—but computed only for night time hours.

6. CONCLUSIONS

In this study, the solar potential over Europe has been assessed, leading to several insights. The analyses show that the regions with the greatest potential for solar power resources lie in southern Europe, at latitudes south of France. In this area, the annual mean solar power is above the threshold for harvestable photovoltaic power as determined by industry standards, with availability above 50%. Other areas of promising resource potential exist in intermediate latitudes, between southern France and southern England, where availability coefficients are around 0.5 and over a considerable portion of the year the mean solar power is still harvestable. These are also the only two areas showing significant antiNullCoincidence, which quantifies the potential for intermittency mitigation via aggregation by measuring the extent to which renewable power generation is available in surrounding regions when not available locally. The highest antiNullCoincidence for solar power is found in France, Spain, Italy, Germany and Greece, and therefore we expect intermittency in these regions to be mitigated the most from interconnection of solar farms. Central European countries also display notable antiNullCoincidence for solar generation, whereas they show complete lack of this parameter for wind power generation.

A secondary aim of this report was to assess the potential benefits of co-location of wind and solar power generation over Europe. Several metrics have been introduced to do so, concluding that wind and solar potentials are anti-correlated at seasonal and monthly timescales, which with co-location increases the availability of power over Europe. For example, we find that through co-location, renewable power generation would be available more than 70% of the time in southern Europe, and more than 50% of the time in the intermediate latitudes of Europe. Our results also show that the Atlantic Ocean shows the highest anti-correlation between wind and solar, and that the impact of wind turbine cut-outs remains negligible. In order to take advantage of the full extent of anti-correlation between wind and solar over the ocean, technologies for harvesting wind power at high speeds must advance to be deployed further in the ocean. Our highest confidence was found inland, in southern Europe and at intermediate latitudes. This is also where the results concerning solar potential and the benefits of co-location of solar and wind powers are the most encouraging. In terms of intermittency, we found that antiNullCoincidence was increased by co-location of wind and solar power generation in the areas where wind power was already displaying this at offshore and coastal locations. We also showed that by combining wind and solar power, antiNullCoincidence may be found in the Mediterranean and Baltic countries, meaning that when one location has no power, at least 50% of the time other locations in the surrounding areas have harvestable power. Finally, we found that areas in central Europe were not benefiting from co-location between wind and solar, but displayed antiNullCoincidence for solar only.

Several limitations to our study are notable. The solar and cloud data used in this study are the product of the assimilation of measurements and satellite-remote sensed data into a global model. Imperfections of the model, the assimilation schemes, and supporting observations can adversely influence the computed output. In addition, due to the spatial resolution of ½° (lat) × ⅔° (lon),

local cloudiness, at the scale of individual wind or solar installations, is not explicitly resolved. The time resolution of the reanalysis output allows for intermittency and other phenomena for timescales of one hour (or longer) to be studied. Furthermore, territorial, economic and deployment landscapes are not taken into consideration. Comparing MERRA cloud data to CM SAF cloud observations, the results showed the weakest consistency over the ocean, Iceland, Ireland and the United Kingdom. Where solar potential is highest, MERRA cloud data matches CM SAF cloud data.

Our study emphasizes that aggregating solar and wind power resources could mitigate intermittency in the Mediterranean coastal countries and the Baltic regions, as well as strengthen the intermittency mitigation where interconnections of wind power installations may already do so. The highest potential benefits of co-located wind and solar power generation can be seen offshore, as well as in fairly remote areas. In these areas, any over-ocean deployment strategy would require further technological advances to deploy turbines where the ocean is deep and their structural resilience can withstand an open-ocean environment. Further, we found that central-eastern Europe countries would benefit most from interconnections of solar-power installations. Future studies on the economic and technical feasibility and efficiency of interconnecting wind and solar farms in these regions are warranted.

Acknowledgments

The authors would like to thank Mr. Hervé Le Treut and Prof. Ronald G. Prinn for providing Mr. Bozonnat the opportunity to work in the MIT Joint Program on the Science and Policy of Global Change. Mr. Bozonnat would also like to thank Alexandra Cosseron for her assistance during the first steps of his internship and Charles Fant for his help with Matlab and for the interesting conversations and suggestions. Mr. Bozonnat would also like to express a special thank you to Adam Schlosser for his sincere and useful guidance and encouragement extended. Finally Mr. Bozonnat would like to thank Maximilien Burq and Emmanuel Siefert for the always valuable and interesting discussions.

REFERENCES

Cano, D., J.M. Monget, M. Albuisson, H. Guillard, N. Regas and L. Wald, 1986: A Method for the Determination of the Global Solar Radiation from Meteorological Satellite Data, *Solar Energy* 37(1), 31-39.

Chenni, R., E. Matagne and M. Khennane, 2011: Study of Solar Radiation in View of Photovoltaic Systems Optimization, *Smart Grid and Renewable Energy,* 2011(2): 367–374.

Conibeer, G., 2007: Third-generation Photovoltaics, *MaterialsToday,* 10,11.

Cosseron, A., C.A. Schlosser and U.B. Gunturu, 2014: Characterization of the Wind Power Resource in Europe and its Intermittency, MIT JPSGPC *Report 258,* March (http://globalchange.mit.edu/files/documents/MITJPSPGC_Rpt258.pdf).

European Commission, 2009: Photovoltaic Solar Energy – Development and Current Research (http://europa.eu).

Gunturu, U.B. and C.A. Schlosser, 2011: Characterization of Wind Power Resource in the United States and its Intermittency, MIT JPSPGC *Report 209*, December, 65p. (http://globalchange.mit.edu/files/documents/MITJPSPGC_Rpt209.pdf).

Hammer, A., D. Heinemann and A. Westerhellweg, 1998: Derivation of Daylight and Solar Irradiance Data from Satellite Observations, *Proceedings of the Ninth Conference on Satellite Meteorology and Oceanography,* Paris, May 1998: 747–50 (http://www.satel-light.com/core.htm).

Hammer, A., D. Heinemann, C. Hoyer, R. Kuhlemann, E. Lorenz, R. Müller and H.G. Beyer, 2003: Solar Energy Assessment Using Remote Sensing Technologies, *Remote Sensing of Environment Journal*.

Heide, D. *et al.*, 2010: Seasonal optimal mix of wind and solar power in a future, highly renewable Europe. In *Renewable Energy (2010),* doi:10.1016/j.renene.2010.03.012.

Huang, X. and S. Han, 2012: Enhancing Solar Cell Efficiency: the search for luminescent materials as spectral converters, *The Royal Society of Chemistry,* 2013(42): 173–201.

Kriesche, P. and C.A. Schlosser, 2014: The Association of Large-Scale Climate Variability and Teleconnections on Wind Energy Resource over Europe and its Intermittency, *Energy Procedia* (in press).

Mueller, R., T. Berehndt, A. Hammer and A. Kemper, 2012: A new algorithm for the satellite-based retrieval of solar surface irradiance in spectral bands. *Remote Sensing* 4(3): 622–647.

Posselt, R., R.W. Mueller, R. Stöckli and J. Trentmann, 2012: Remote sensing of solar surface radiation for climate monitoring – the CM-SAF retrieval in international comparison. *Remote Sensing of Environment* 118: 186–198.

Rienecker, M. M., M.J. Suarez, R. Gelaro, R. Todling, J. Bacmeister, E. Liu, M.G. Bosilovich, S.D. Schubert, L. Takacs, G. Kim, S. Bloom, J. Chen, D. Collins, A. Conaty, A. Da Silva, W. Gu, J. Joiner, R.D. Koster, R. Lucchesi, A. Molod, T. Owens, S. Pawson, P. Pegion, C.R. Redder, R. Reichle, F.R. Robertson, A.G. Ruddick, M. Sienkiewicz and J. Woolen, 2011: MERRA – NASA's Modern-Era Retrospective Analysis for Research and Applications, *J. Climate*, 24.

Suri, M. and J. Hofierka, 2004: A New GIS-based Solar Radiation Model and Its Application to Photovoltaic Assessments, *Trans. GIS,* 8: 175–190.

Suri, M., T.A. Huld and E.D. Dunlop, 2005: PV-GIS: a Web-based Solar Radiation Database for the Calculation of PV Potential in Europe, *International Journal of Sustainable Energy,* 24(2, June): 55–67.

Suri, M., T.A. Huld, E.D. Dunlop and H.A. Ossenbrink, 2007: Potential of Solar Electricity Generation in the European Union Member States and Candidate Countries, *Solar Energy,* 81(2007): 1295–1305.

Ubertini, S. and U. Desideri, 2002: Performance estimation and experimental measurements of a photovoltaic roof, *Renewable Energy,* 28(2003): 1833–1850 (http://www.elsevier.com/locate/renene).

REPORT SERIES of the MIT Joint Program on the Science and Policy of Global Change

FOR THE COMPLETE LIST OF JOINT PROGRAM REPORTS: http://globalchange.mit.edu/pubs/all-reports.php

227. Impacts of Land-Use and Biofuels Policy on Climate: *Temperature and Localized Impacts*. *Hallgren et al.,* August 2012

228. Carbon Tax Revenue and the Budget Deficit: *A Win-Win-Win Solution?* *Rausch and Reilly,* August 2012

229. CLM-AG: An Agriculture Module for the Community Land Model version 3.5. *Gueneau et al.,* September 2012

230. Quantifying Regional Economic Impacts of CO_2 Intensity Targets in China. *Zhang et al.,* September 2012

231. The Future Energy and GHG Emissions Impact of Alternative Personal Transportation Pathways in China. *Kishimoto et al.,* September 2012

232. Will Economic Restructuring in China Reduce Trade Embodied CO_2 Emissions? *Qi et al.,* October 2012

233. Climate Co-benefits of Tighter SO_2 and NO_x Regulations in China. *Nam et al.,* October 2012

234. Shale Gas Production: *Potential versus Actual GHG Emissions*. *O'Sullivan and Paltsev,* November 2012

235. Non-Nuclear, Low-Carbon, or Both? *The Case of Taiwan*. *Chen,* December 2012

236. Modeling Water Resource Systems under Climate Change: *IGSM-WRS*. *Strzepek et al.,* December 2012

237. Analyzing the Regional Impact of a Fossil Energy Cap in China. *Zhang et al.,* January 2013

238. Market Cost of Renewable Jet Fuel Adoption in the United States. *Winchester et al.,* January 2013

239. Analysis of U.S. Water Resources under Climate Change. *Blanc et al.,* February 2013

240. Protection of Coastal Infrastructure under Rising Flood Risk. *Lickley et al.,* March 2013

241. Consumption-Based Adjustment of China's Emissions-Intensity Targets: *An Analysis of its Potential Economic Effects*. *Springmann et al.,* March 2013

242. The Energy and CO_2 Emissions Impact of Renewable Energy Development in China. *Zhang et al.,* April 2013

243. Integrated Economic and Climate Projections for Impact Assessment. *Paltsev et al.,* May 2013

244. A Framework for Modeling Uncertainty in Regional Climate Change. *Monier et al.,* May 2013

245. Climate Change Impacts on Extreme Events in the United States: An Uncertainty Analysis. *Monier and Gao,* May 2013

246. Probabilistic Projections of 21st Century Climate Change over Northern Eurasia. *Monier et al.,* July 2013

247. What GHG Concentration Targets are Reachable in this Century? *Paltsev et al.,* July 2013

248. The Energy and Economic Impacts of Expanding International Emissions Trading. *Qi et al.,* August 2013

249. Limited Sectoral Trading between the EU ETS and China. *Gavard et al.,* August 2013

250. The Association of Large-Scale Climate Variability and Teleconnections on Wind Resource over Europe and its Intermittency. *Kriesche and Schlosser,* September 2013

251. Regulatory Control of Vehicle and Power Plant Emissions: *How Effective and at What Cost?* *Paltsev et al.,* October 2013

252. Synergy between Pollution and Carbon Emissions Control: *Comparing China and the U.S.* *Nam et al.,* October 2013

253. An Analogue Approach to Identify Extreme Precipitation Events: *Evaluation and Application to CMIP5 Climate Models in the United States*. *Gao et al.* November 2013

254. The Future of Global Water Stress: *An Integrated Assessment*. *Schlosser et al.,* January 2014

255. The Mercury Game: *Evaluating a Negotiation Simulation that Teaches Students about Science–Policy Interactions*. *Stokes and Selin,* January 2014

256. The Potential Wind Power Resource in Australia: *A New Perspective*. *Hallgren et al.,* February 2014

257. Equity and Emissions Trading in China. *Zhang et al.,* February 2014

258. Characterization of the Wind Power Resource in Europe and its Intermittency. *Cosseron et al.,* March 2014

259. A Self-Consistent Method to Assess Air Quality Co-Benefits from US Climate Policies. *Saari et al.,* April 2014

260. Electricity Generation and Emissions Reduction Decisions under Policy Uncertainty: *A General Equilibrium Analysis*. *Morris et al.,* April 2014

261. An Integrated Assessment of China's Wind Energy Potential. *Zhang et al.,* April 2014

262. The China-in-Global Energy Model. *Qi et al.* May 2014

263. Markets versus Regulation: *The Efficiency and Distributional Impacts of U.S. Climate Policy Proposals*. *Rausch and Karplus,* May 2014

264. Expectations for a New Climate Agreement. *Jacoby and Chen,* August 2014

265. Coupling the High Complexity Land Surface Model ACASA to the Mesoscale Model WRF. *Xu et al.,* August 2014

266. The CO_2 Content of Consumption Across US Regions: *A Multi-Regional Input-Output (MRIO) Approach*. *Caron et al.,* August 2014

267. Carbon emissions in China: *How far can new efforts bend the curve?* *Zhang et al.,* October 2014

268. Characterization of the Solar Power Resource in Europe and Assessing Benefits of Co-Location with Wind Power Installations. *Bozonnat and Schlosser,* October 2014

Contact the Joint Program Office to request a copy. The Report Series is distributed at no charge.